ACS APPLIED MATERIALS & INTERFACES

Letter

www.acsami.org

Biomorphic Synthesis of Mesoporous Co_3O_4 Microtubules and Their Pseudocapacitive Performance

Dongliang Yan,*[,†] Huan Zhang,[†] Lin Chen,*[,‡] Guisheng Zhu,[†] Shichao Li,[†] Huarui Xu,*[,†] and Aibing Yu[§]

[†]Guangxi Key Laboratory of Information Materials, Guilin University of Electronic Technology, Guilin 541004, P.R. China

[‡]Department of Material and Chemistry Engineering, Pingxiang University, Pingxiang 337055, P.R. China

[§]Department of Chemical Engineering, Monash University, Clayton, Victoria 3800, Australia

Supporting Information

ABSTRACT: A novel meosoporous tubular Co_3O_4 has been fabricated by a simple and cost-effective biomorphic synthesis route, which consists of infiltration of cotton fiber with cobalt nitrate solution and postcalcination at 673 K for 1 h. Its electrochemical performance as a supercapacitor electrode material is investigated by means of cyclic voltammetry and chronopotentiometry tests. Compared with bulk Co_3O_4 prepared without using cotton template, biomorphic Co_3O_4 displays 2.8 fold enhancement of pseudocapacitive performance because of the unique tubular morphology, relative high specific surface area (3 and 0.8 m^2/g for biomorphic Co_3O_4 and bulk Co_3O_4, respectively), and mesoporous nature.

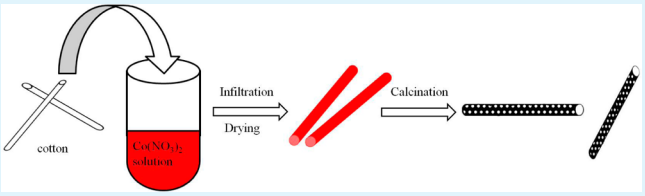

KEYWORDS: *biomorphic, energy storage and conversion, mesoporous, pseudocapacitive performance*

Cobalt oxide (Co_3O_4) is an important functional material used in a wide range of applications in lithium-ion batteries, supercapacitors, gas sensing, catalysis, and electro-chromic devices because of its structural flexibility and distinctive physical and chemical properties.[1−6] Because eof the influence of morphology on the performance of materials, numerous studies have been undertaken to prepare Co_3O_4 with different morphologies, such as flowers,[7] sheets,[8] boxes,[9] twin-sphere,[10] wires,[11,12] rods,[13] and tubes.[1] Among these microstructures, one-dimensional tubular materials with diameters ranging from micro- to nanoscale through template techniques is more attractive because of their remarkable physicochemical properties and potential applications. For example, Yagmur et al.[14] prepared Co_3O_4 nanotubes on nickel foam templated from porous anodic aluminum oxide and demonstrated a superior pseudocapacitive performance could be achieved. On the other hand, Li et al.[1] reported the fabrication of Co_3O_4 microtubes by a porous-alumina-template method and their excellent lithium storage properties. Cobalt oxide nanotubes were also synthesized by calcining cobalt nanowires embedded in an anodic alumina template.[15] However, most of the above methods are too complex and expensive to be used in a versatile or environmentally friendly manner.

In recent years, using natural biomaterials such as paper,[16] wood,[17] cotton,[18−20] egg shell membranes,[21] sorghum straw,[22] butterfly wing,[23,24] pollen grain,[25] legume,[26] and microalgae[27] as templates to fabricate biomorphic advanced functional materials has been more attractive. Compared with man-made template materials, natural biomaterials display a hierarchically built structures owing to their long-term genetic evolution and optimization, and are also abundant, diverse, cheap, and reproducible.[16,28] Interestingly, several researchers employed this novel strategy to prepare 1D tubular materials. For instance, Fan and co-workers prepared Al_2O_3 microtubes by replicating the cotton fibers.[29] Biomorphic synthesis of ZnO hollow fibers and birnessite MnO_2 tubes were also studied by Su et al.[28] and Yan et al.,[18] respectively. Biomorphic MoO_3[30] and $LaFeO_3$[31] microtubules were also fabricated using cotton as biotemplates by Song group. To the best of our knowledge, however, there have been no reports on the synthesis of tubelike Co_3O_4 by a biotemplate process.

Here, we report the preparation of biomorphic Co_3O_4 microtubes with mesoporous structure by using cotton as biotemplates. The pseudocapacitive performances of the as-obtained samples were investigated. Benefiting from unique tubular morphology, high specific surface area, and mesoporous nature, biomorphic Co_3O_4 exhibits 2.8 times specific capacitance of a bulk sample.

The morphologies of the as-prepared samples are first examined by SEM as shown in Figure 1. SEM images display that the product prepared using cotton as the template has a tubular morphology (Figure 1b, c), which is very close to that of cotton (Figure 1a). Obviously, the as-obtained Co_3O_4 inherits the morphology of cotton and exhibits a biomorphic structure. Without cotton, only irregular Co_3O_4 particles were obtained (Figure 1d).

Figure 2a displays the XRD patterns of the biomorphic and bulk Co_3O_4. The XRD patterns of both products match well with the standard XRD pattern of face-centered cubic phase of Co_3O_4

Received: July 9, 2014
Accepted: September 10, 2014
Published: September 10, 2014

   dx.doi.org/10.1021/am5044449 | ACS Appl. Mater. Interfaces 2014, 6, 15632−15637

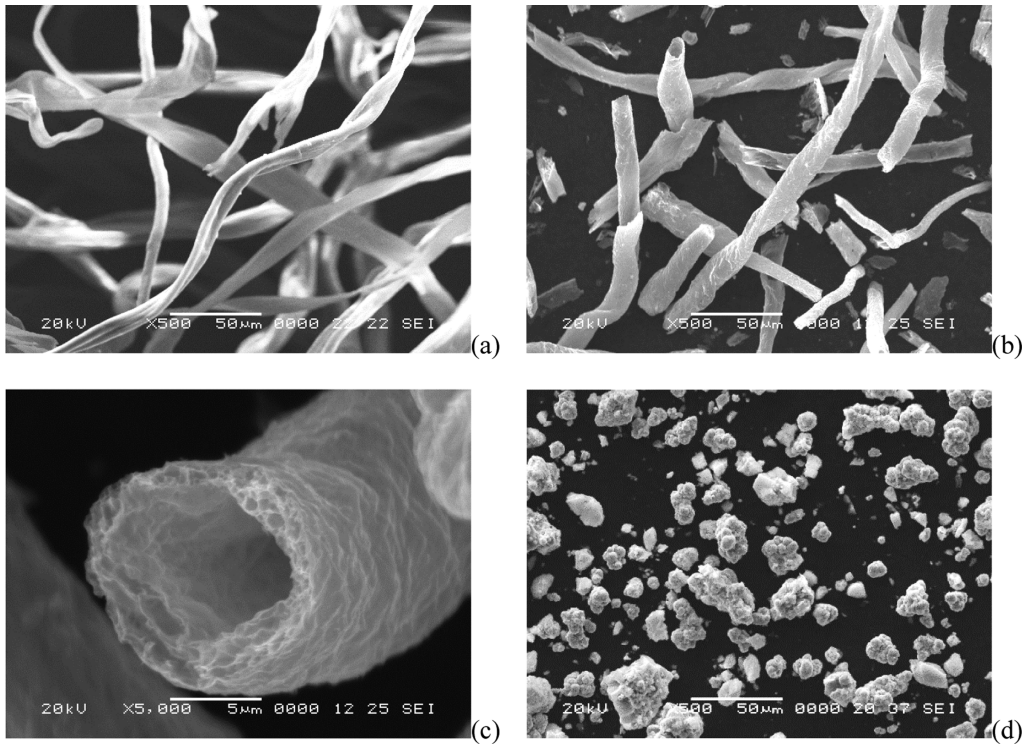

Figure 1. SEM images of (a) cotton, (b) biomorphic Co_3O_4 (low magnification), (c) biomorphic Co_3O_4 (high magnification), (d) bulk Co_3O_4.

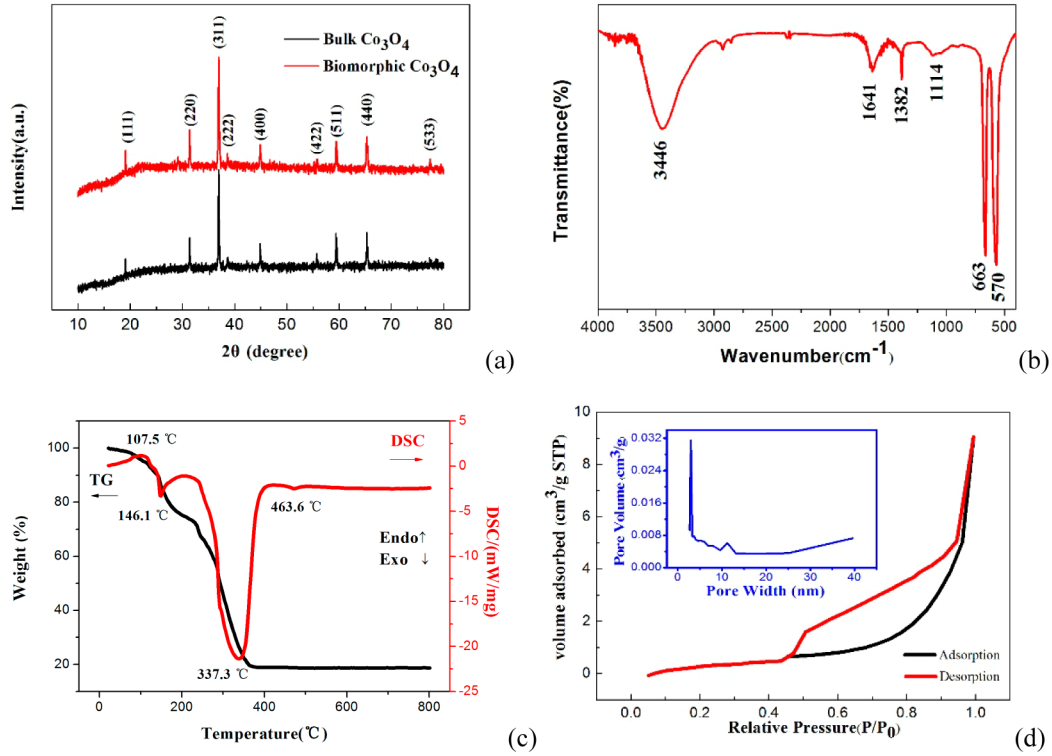

Figure 2. (a) XRD patterns of biomorphic Co_3O_4 and bulk Co_3O_4, (b) FT-IR spectrum, (c) TG-DSC curve, and (d) N_2 adsorption−desorption and pore size distribution (inset) curves for biomorphic Co_3O_4.

(JCPDS 42−1467).[1,7] The lattice constants were calculated to be $a = b = c = 0.8090$ nm and $a = b = c = 0.8087$ nm for the bulk and biomorphic Co_3O_4, respectively, both of them are consistent with the standard values of Co_3O_4 ($a = b = c = 0.8083$ nm). FT-IR spectrum (Figure 2b) was analyzed to further identify the structure of the biomorphic Co_3O_4. The vibration frequencies at 663 and 570 cm^{-1} confirm the formation of Co_3O_4 with a spinel structure.[32,33] The vibration frequencies at 3446, 1641, 1382, and 1114 cm^{-1} are assigned to the O−H stretching, relating to adsorbed water in the product.[29,34]

TG-DSC analysis was performed on the infiltrated samples to trace the formation of biomorphic Co_3O_4 (Figure 2c). A broad

dx.doi.org/10.1021/am5044449 | ACS Appl. Mater. Interfaces 2014, 6, 15632−15637

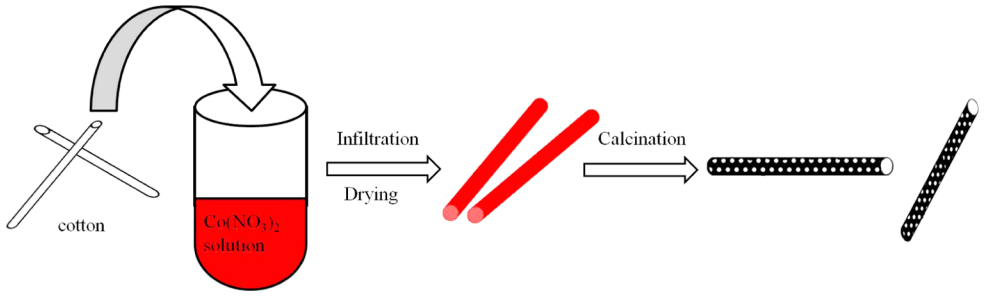

Figure 3. Illustration of the mechanism of formation of Co_3O_4 sample.

endothermic peak, accompanied by a weight loss of 11% in TG, was observed at 107.5 °C. This could be ascribed to the desorption of physically adsorbed water. Around 146.1 °C, an exothermic peak occurred with 18.1% weight loss between 146 and 234 °C because of the decomposition of cobaltous (II) nitrate hexahydrate. The two other exothermic peaks were found at around 337.3 and 463.6 °C accompanied by a weight loss of 53.2% in the temperature range of 237 to 520 °C, which is ascribed to the burn-out of the cotton fibers.[18,29]

On the basis of the above results, a possible three-step formation mechanism of tubular Co_3O_4 was proposed (Figure 3). When the cotton fiber was immersed into the precursor solution, the water and $Co(NO_3)_2$ molecules were absorbed onto the hydroxyl-group-rich substrate of the cotton fibers through hydrogen bonds, coordination bonds, or the van der Waals forces.[35] As heat treatment temperature was increased to about 150 °C, thermal decomposition of $Co(NO_3)_2{\cdot}6H_2O$ occurred[32]

$$3Co(NO_3)_2{\cdot}6H_2O \xrightarrow{\Delta} Co_3O_4 + O_2\uparrow + 6NO_2\uparrow + 18H_2O\uparrow \quad (1)$$

When the calcinating temperature was further elevated, the precise replication of cotton texture could be achieved after the removal of the organic substance.

The nitrogen adsorption−desorption isotherms and corresponding pore size distribution of the biomorphic Co_3O_4 are shown in Figure 2d. The isotherms shape exhibits the type IV isotherm with a type H3 hysteresis loop, suggesting the presence of mesopores in the product. Biomorphic Co_3O_4 shows that the pore size distribution is in the range of 9−13 nm. The average pore diameter is 5 nm. The specific surface area of biomorphic Co_3O_4 is 3.0 m^2/g, much larger than that of bulk Co_3O_4 (0.8 m^2/g). The high surface area and the mesopore structure is beneficial to the contact of the electrolytes with the active materials, which can further increase the electrochemical properties.[2−9,37]

Cyclic voltammograms test for biomorphic (red) and bulk (black) Co_3O_4 were recorded under the same conditions and shown in Figure 4a. The enclosed area of a CV curve for biomorphic Co_3O_4 is obviously larger than that for bulk Co_3O_4, suggesting that biomorphic Co_3O_4 has a high specific capacitance than bulk Co_3O_4. Figure 4b shows the CV of the biomorphic Co_3O_4 test in the potential window from 0 to 0.45 V (vs SCE) at the different scant rates. Two pairs of redox peaks can be found at a low scan rate (5 mV s^{-1}), which correspond to the conversion between different cobalt oxidation states according the following equations[2,8−10]

$$Co_3O_4 + OH^- + H_2O \Leftrightarrow 3CoOOH + e^- \quad (2)$$

$$CoOOH + OH^- \Leftrightarrow CoO_2 + H_2O + e^- \quad (3)$$

When increasing the scan rate, peak currents were also increased, indicating good reversibility of the fast charge−discharge response of the materials.[8−10]

Galvanostatic charge−discharge performance of biomorphic and bulk Co_3O_4 in the potential range of 0 to 0.45 V are exhibited in Figure 4c, d. Figure 4c clearly shows that the discharging time of biomorphic Co_3O_4 (red) became much longer than that of bulk Co_3O_4 (black). The specific capacitances of biomorphic Co_3O_4 and bulk Co_3O_4 at 0.5 A g^{-1} are 130.5 F g^{-1} and 46.0 F g^{-1}, respectively, suggesting a 2.8 fold improvement over the bulk Co_3O_4. On the basis of the results of Figure 4d, the specific capacitance of biomorphic Co_3O_4 is 128.3, 124.6, and 119.0 F g^{-1} at the current densities of 1, 1.5, and 2 A g^{-1} respectively. The current density dependence of the specific capacitance of the electrode is exhibited in Figure 4e.

The superior electrochemical properties of the biomorphic Co_3O_4 can be further demonstrated by the electrochemical impedance spectroscopy (EIS). Figure 4f compares the Nyquist plots of the biomorphic Co_3O_4 with that of bulk Co_3O_4. All EIS curves are composed of a semicircle in high frequency regions and a straight slopping line in low frequency regions. Such a pattern of the EIS can be fitted by an equivalent circuit displayed in the inset of Figure 4f, where R_s, C_{dl}, Z_W, R_{ct}, and C_F represent the solution resistance (internal resistances), a double layer capacitor, a finite-length Warbury diffusion element, Co_3O_4-electrolyte interfacial charge transfer resistance and a faradic pseudocapacitor, respectively.[38] It is noted that biomorphic Co_3O_4 exhibits a smaller semicircle at the high frequency region, indicating that biomorphic Co_3O_4 has a smaller charge transfer resistance.[2−9,38,39] At the low frequency region, a more vertical straight line of biomorphic Co_3O_4 was observed compared to the bulk Co_3O_4, which is further evidence for the fast ion diffusion behavior of the biomorphic Co_3O_4 electrode.[40] These results confirm that the biomorphic Co_3O_4 can provide a convenient pathway for the ion and electron transport, which are consistent with the capacitive results above.

The long-term cycling test of biomorphic Co_3O_4 was performed by charge−discharge technique at a current density of 1 A g^{-1}, as shown in Figure 4g. After 3000 cycles, only 8.3% capacitance fade was found, suggesting the excellent cyclic stability of the electrode. We attributed the improved electrochemical performance of biomorphic Co_3O_4 to their unique tubular morphology, relative high specific surface area and mesoporous nature.

In summary, a simple and cost-effective biomorphic synthesis route has been developed to prepare Co_3O_4 microtubules using cotton as biotemplates. The as-prepared sample inherits the morphology and microstructure of cotton. The biomorphic Co_3O_4 displays improved electrochemical performance bene-

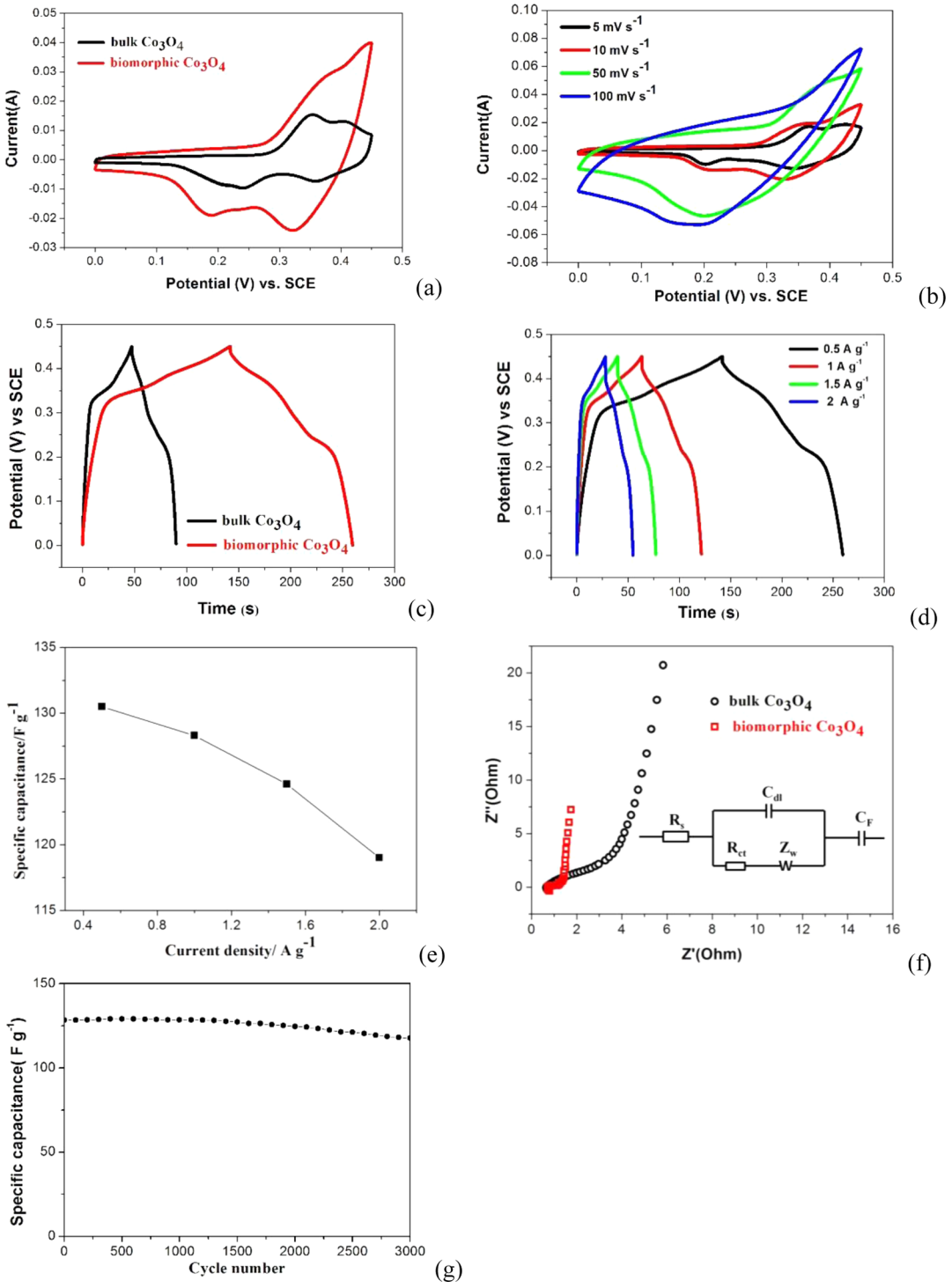

Figure 4. (a) Comparison of cyclic voltammograms curves at 10 mV s^{-1} for biomorphic (red) and bulk (black) Co_3O_4. (b) Cyclic voltammograms curves at different scan rates for biomorphic Co_3O_4. (c) Comparison of galvanostatic charge−discharge curves at 0.5 A g^{-1} for biomorphic (red) and bulk (black) Co_3O_4. (d) Galvanostatic charge−discharge curves at different current density for biomorphic Co_3O_4. (e) Specific capacitance as a function of current density. (f) Comparison of Nyquist plots for biomorphic (red) and bulk (black) Co_3O_4 (the inset is the equivalent circuit). (g) Cycling performance for biomorphic Co_3O_4 during 3000 cycles.

fited from its unique tubular morphology, relative high specific surface area, and mesoporous nature.

■ ASSOCIATED CONTENT

Ⓢ Supporting Information

Experimental details (PDF). This material is available free of charge via the Internet at http://pubs.acs.org.

■ AUTHOR INFORMATION

Corresponding Authors

*E-mail: dlyan@guet.edu.cn. Tel.: +86 773 2291159. Fax: +86 773 2191903.
*E-mail: rymw27@163.com.
*E-mail: huaruixu@guet.edu.cn.

Notes

The authors declare no competing financial interest.

■ ACKNOWLEDGMENTS

We acknowledge the financial support from the National Natural Science Foundation of China (21176051 and 61166008), Guangxi Natural Science Foundation (2012GXNSFFA060002, 2013GXNSFAA019294, and 2013GXNSFBA019234), and Department of Education of Jiangxi Province in China (GJJ14787). This work was jointly sponsored by Guangxi Key Laboratory of Information Materials at Guilin University of Electronic Technology in China (with Grants 1110908-02-K and 1110908-05-K), State Key Laboratory of Advanced Technology for Materials Synthesis and Processing at Wuhan University of Technology in China (2012-KF-7), and Guangxi Experiment Center of Information Science at Guilin University of Electronic Technology in China (20130322).

■ REFERENCES

(1) Li, W. Y.; Xu, L. N.; Chen, J. Co_3O_4 Nanomaterials in Lithium-ion Batteries and Gas Sensors. *Adv. Funct. Mater.* **2008**, *15*, 851−857.

(2) Yuan, C. Z.; Yang, L.; Hou, L. R.; Li, J. Y.; Sun, Y. X.; Zhang, X. G.; Shen, L. F.; Lu, X. J.; Xiong, S. L.; Lou, X. W. Flexible Hybrid Paper Made of Monolayer Co_3O_4 Microsphere Arrays on rGO/CNTs and Their Application in Electrochemical Capacitors. *Adv. Funct. Mater.* **2012**, *22*, 2560−2566.

(3) Kuo, C. H.; Li, W. K.; Song, W. Q.; Luo, Z.; Poyraz, A. S.; Guo, Y.; Ma, W. K.; Suib, S. L.; He, J. Facile Synthesis of Co_3O_4@CNT with High Catalytic Activity for CO Oxidation under Moisture-Rich Conditions. *ACS Appl. Mater. Interfaces* **2014**, *6*, 11311−1317.

(4) Hou, L. R.; Yan, C. Z.; Yang, L.; Sheng, L. F.; Zhang, F.; Zhang, X. G. Urchin-Like Co3O4Microspherical Hierarchical Superstrutures Constructed by One-dimension Nanowires Toward Electrochemical Capacitors. *RSC Adv.* **2011**, *1*, 1521−1526.

(5) Liu, M. C.; Kong, L. B.; Lu, C.; Li, X. M.; Luo, Y. C.; Kang, L. A Sol-Gel Process for Fabrication of $NiO/NiCo_2O_4/Co_3O_4$ Composite with Improved Electrochemical Behavior for Electrochemical Capacitors. *ACS Appl. Mater. Interfaces* **2012**, *4*, 4631−4636.

(6) Peterson, G. R.; Low, F. H.; Gumeci, C.; Bassett, W. P.; Korzeniewski, C.; Weeks, L. S. Preparation-Morphology-Performance Relationships in Cobalt Aerogels as Supercapacitors. *ACS Appl. Mater. Interfaces* **2014**, *6*, 1796−1803.

(7) Rui, X. H.; Tan, H. T.; Sim, D. H.; Liu, W. L.; Xu, C.; Hng, H. H.; Yazami, R.; Lim, T. M.; Yan, Q. Y. Template-free Synthesis of Urchin-like Co_3O_4 Hollow Spheres with Good Lithium Storage Properties. *J. Power Sources* **2013**, *222*, 97−102.

(8) Yuan, C. Z.; Yang, L.; Hou, L. R.; Shen, L. F.; Zhang, X. G.; Lou, X. W. Growth of Ultrathin Mesoporous Co_3O_4 Nanosheet Arrays on Ni Foam for High-performance Electrochemical Capacitors. *Energy Environ. Sci.* **2012**, *5*, 7883−7887.

(9) Du, W.; Liu, R. M.; Jiang, Y. W.; Lu, Q. Y.; Fan, Y. Z.; Gao, F. Facile Synthesis of Hollow Co_3O_4 Boxes for High Capacity Supercapacitor. *J. Power Sources* **2013**, *227*, 101−105.

(10) Xiao, Y. H.; Liu, S. J.; Li, F.; Zhang, A. Q.; Zhao, J. H.; Fang, S. M.; Jia, D. Z. 3D Hierarchical Co_3O_4 Twin-Spheres with an Urchin-Like Structure: Large-Scale Synthesis, Multistep-Splitting Growth, and Electrochemical Pseudocapacitors. *Adv. Funct. Mater.* **2012**, *22*, 4052−4059.

(11) Li, Y. G.; Tan, B.; Wu, Y. Y. Freestanding Mesoporous Quasi-Single-Crystalline Co_3O_4 Nanowire Arrays. *J. Am. Chem. Soc.* **2006**, *128*, 14258−14259.

(12) Yang, Q.; Lu, Z. Y.; Chang, Z.; Zhu, W.; Sun, J. Q.; Liu, J. F.; Sun, X. M.; Duan, X. Hierarchical Co_3O_4 Nanosheet@Nanowire Arrays with Enhanced Pseudocapacitive Performance. *RSC Adv.* **2012**, *2*, 1663−1668.

(13) Xie, X. W.; Shen, W. J. Morphology Control of Cobalt Oxide Nanocrystals for Promoting Their Catalytic Performance. *Nanoscale* **2009**, *19*, 50−60.

(14) Yagmur, V.; Atalay, F. E.; Kaya, H.; Avcu, D.; Aydogmus, E. Electrochemical Capacitance of Cobalt Oxide Nanotubes on Nickel Foam. *Acta Phys. Polym., A* **2013**, *123*, 215−217.

(15) Li, T.; Yang, S. G.; Huang, L. S.; Gu, B. X.; Du, Y. W. A Novel Process from Cobalt Nanowire to Co_3O_4 Nanotube. *Nanotechnology* **2004**, *15*, 1479−1482.

(16) Li, J.; Kwong, F. L.; Ng, D. H. L. Synthesis of a Biomorphic Molybdenum Trioxide Templated from Paper. *J. Am. Ceram. Soc.* **2008**, *91*, 1350−1353.

(17) Liu, Z. T.; Fan, T. X.; Zhang, D. Synthesis of Biomorphous Nickel Oxide from a Pinewood Template and Investigation on a Hierarchical Porous Structure. *J. Am. Ceram. Soc.* **2006**, *89*, 662−665.

(18) Yan, D. L.; Li, S. C.; Zhu, G. S.; Wang, Z. M.; Xu, H. R.; Yu, A. B. Synthesis and Pseudocapacitive Behaviors of Biomorphic Mesoporous Tubular MnO_2 Templated from Cotton. *Mater. Lett.* **2013**, *95*, 164−167.

(19) Song, P.; Wang, Q.; Yang, Z. X. Biomorphic Synthesis of $ZnSnO_3$ Hollow Fibers for Gas Sensing Application. *Sens. Actuators, B* **2011**, *156*, 983−989.

(20) Song, P.; Wang, Q.; Yang, Z. X. Biomorphic Synthesis and Gas Response of In_2O_3 Microtubules Using Cotton Fibers as Templates. *Sens. Actuators, B* **2012**, *168*, 421−428.

(21) Dong, Q.; Su, H. L.; Song, F.; Zhang, D.; Wang, N. Hierarchical Metal Oxides Assembled by Nanocrystallites via a Simple Bio-inspired Route. *J. Am. Ceram. Soc.* **2007**, *90*, 376−380.

(22) Song, P.; Zhang, H. H.; Han, D.; Li, J.; Yang, Z. X.; Wang, Q. Preparation of Biomorphic Porous $LaFeO_3$ by Sorghum Straw Biotemplate Method and Its Acetone Sensing Properties. *Sens. Actuators, B* **2014**, *196*, 140−146.

(23) Weatherspoon, M. R.; Cai, Y.; Crne, M.; Srinivasarao, M.; Sandhage, K. H. 3D Rutile Titania-Based Structures with *Morpho* Butterfly Wing Scale Morphologies. *Angew. Chem., Int. Ed.* **2008**, *47*, 7921−7923.

(24) Hang, J. Y.; Wang, X. D.; Wang, Z. L. Controlled Replication of Butterfly Wings for Achieving Tunable Photonic Properties. *Nano Lett.* **2006**, *6*, 2325−2331.

(25) Hall, S. R.; Bolger, H.; Mann, S. Morphosynthesis of Complex Inorganic Forms Using Pollen Grain Templates. *Chem. Commun.* **2003**, 2784−2785.

(26) Zhao, Y. F.; Wei, M.; Lu, J.; Wang, Z. L.; Duan, X. Biotemplated Hierarchical Nanostructure of Layered Double Hydroxides with Improved Photocatalysis Performance. *ACS Nano* **2009**, *3*, 4009−4016.

(27) Tao, X. Y.; Wu, R.; Xia, Y.; Huang, H.; Chai, W. C.; Feng, T.; Gan, Y. P.; Zhang, W. K. Biotemplated Fabrication of Sn@C Anode Materials Based on the Unique Metal Biosorption Behavior of Microalgae. *ACS Appl. Mater. Interfaces* **2014**, *6*, 3696−3702.

(28) Su, B. T.; Wang, K.; Dong, N.; Mu, H. M.; Lei, Z. Q.; Tong, Y. C.; Bai, J. Biomorphic Synthesis of Long ZnO Hollow Fibers with Porous Walls. *J. Mater. Process. Technol.* **2009**, *209*, 4088−4092.

(29) Fan, T. X.; Sun, B. H.; Gu, J. J.; Zhang, D.; Lau, L. W. M. Biomorphic Al_2O_3 Fibers Synthesized Using Cotton as Bio-templates. *Scr. Mater.* **2005**, *53*, 893−897.

(30) Song, P.; Wang, Q.; Li, J.; Yang, Z. X. Morphology-Controllable Synthesis, Characterization and Sensing Properties of Single-Crystal Molybdenum Trioxide. *Sens. Actuators, B* **2013**, *181*, 620−628.

(31) Song, P.; Wang, Q.; Zhang, Z.; Yang, Z. X. Synthesis and Gas Sensing Properties of Biomorphic $LaFeO_3$ Hollow Fibers Templated from Cotton. *Sens. Actuators, B* **2010**, *147*, 248−254.

(32) Tong, G. X.; Liu, Y.; Guan, J. G. In Situ Gas Bubble-Assisted One-Step Synthesis of Polymorphic Co_3O_4 Nanostructures with Improved Electrochemical Performance for Lithium Ion Batteries. *J. Alloys Compd.* **2014**, *601*, 167−174.

(33) He, T.; Chen, D. R.; Jiao, X. L.; Wang, Y. L.; Duan, Y. Z. Solubility-Controlled Synthesis of High-Quality Co_3O_4 Nanocrystals. *Chem. Mater.* **2005**, *17*, 4023−4030.

(34) Yan, D. L.; Zhang, H.; Li, S. C.; Zhu, G. S.; Wang, Z. M.; Xu, H. R.; Yu, A. B. Formation of Ultrafine Three-Dimensional Hierarchical Birnessite-Type MnO_2 Nanoflowers for Supercapacitor. *J. Alloys Compd.* **2014**, *607*, 245−250.
(35) Yan, D. L.; Guo, Z. L.; Zhu, G. S.; Yang, H. J.; Wei, R. H.; Xu, H. R.; Yu, A. B. Electrochemical Properties of 3D MnO_2 Film Prepared by Chemical Bath Deposition at Room Temperature. *Mater. Lett.* **2012**, *82*, 156−158.
(36) Cui, Z. K.; Liu, J.; Zeng, D. W.; Liu, H. W.; Xie, C. S. Quasi-One-Dimensional Bismuth Tungsten Oxide Nanostructures Templated by Cotton Fibers. *J. Am. Ceram. Soc.* **2010**, *93*, 1479−1483.
(37) Yan, D. L.; Guo, Z. L.; Zhu, G. S.; Yu, Z. Z.; Xu, H. R.; Yu, A. B. MnO_2 Film with Three-Dimensional Structure Prepared by Hydrothermal Process for Supercapacitor. *J. Power Sources* **2012**, *199*, 409−412.
(38) Hou, L. R.; Lin, L.; Li, D. K.; Pang, G.; Li, J. F.; Zhang, X. G.; Xiong, S. L.; Yuan, C. Z. Mesoporous N-Containing Carbon Nanosheets Towards High-Performance Electrochemical Capacitors. *Carbon* **2013**, *64*, 141−149.
(39) Yan, D. L.; Zhang, H.; Chen, L.; Zhu, G. S.; Wang, Z. M.; Xu, H. R.; Yu, A. B. Supercapacitive Properties of Mn_3O_4 Nanoparticles Bio-Synthesized from Banana Peel Extract. *RSC Adv.* **2014**, *4*, 23649−23652.
(40) Jeong, J. J.; Choi, B. G.; Lee, S. C.; Lee, K. G.; Chang, S. J.; Han, Y. K.; Lee, Y. B.; Lee, H. U.; Kwon, S.; Lee, G. H. Hierarchical Hollow Spheres of Fe_2O_3@Polyaniline for Lithium Ion Battery Anodes. *Adv. Mater.* **2013**, *25*, 6250−6255.